Article

PtSnIr/C Anode Electrocatalysts: Promoting Effect in Direct Ethanol Fuel Cells

Júlio C. M. Silva,[a] Rodrigo F. B. De Souza,[a] Mayara A. Romano,[a] Melina D'Villa-Silva,[a]
Marcelo L. Calegaro,[b] Peter Hammer,[c] Almir O. Neto[d] and Mauro C. Santos*,[a]

[a]*Laboratório de Eletroquímica e Materiais Nanoestruturados, Centro de Ciências Naturais e Humanas,*
Universidade Federal do ABC, Rua Santa Adélia, 166, 09210-170 Santo André-SP, Brazil

[b]*Grupo de Materiais Eletroquímicos e Métodos Eletroanalíticos, Instituto de Química de São Carlos,*
Universidade de São Paulo, CP 780, 13566-590 São Carlos-SP, Brazil

[c]*Instituto de Química, Universidade Estadual de São Paulo, 14800-060 Araraquara-SP, Brazil*

[d]*Instituto de Pesquisas Energéticas e Nucleares-Comissão Nacional de Energia Nuclear (IPEN-CNEN),*
Av. Prof. Lineu Prestes, 2242, 05508-900 São Paulo-SP, Brazil

Este estudo investiga o efeito promotor de anodos eletrocatalisadores do tipo PtSnIr/C (1:1:1), preparados pelo método de precursor polimérico, na reação de oxidação de etanol em uma célula a combustível de etanol direto (DEFC). Todos os materiais usados foram metal 20% m/m com relação a carbono. Análise por espectroscopia fotoelétrica de raios X (XPS) mostrou a presença de Pt, $PtOH_2$, PtO_2, SnO_2 e IrO_2 na superfície do eletrocalisador, indicando uma possível estrutura de partícula revestida. Análise por difratometria de raios X (XRD) indicou Pt e Ir metálicos assim como a formação de uma liga com Sn. Utilizando eletrocatalisadores do tipo PtSnIr/C preparados para este estudo com quantidades de Pt duas vezes menor que em eletrocatalisadores do tipo PtSn/C E-tek, foi possível obter a mesma densidade de potência máxima encontrada para o material comercial. O produto de reação principal foi ácido acético provavelmente devido a presença de óxidos, neste caso o mecanismo bifuncional é predominante, mas um efeito eletrônico não deve ser descartado.

This study investigates the promoting effect of PtSnIr/C (1:1:1) electrocatalyst anode, prepared by polymeric precursor method, on the ethanol oxidation reaction in a direct ethanol fuel cell (DEFC). All of the materials used were 20% metal m/m on carbon. X-ray photoelectron spectroscopy (XPS) analysis showed the presence of Pt, $PtOH_2$, PtO_2, SnO_2 and IrO_2 at the electrocatalyst surface, indicating a possible decorated particle structure. X-ray diffractometry (XRD) analysis indicated metallic Pt and Ir as well as the formation of an alloy with Sn. Using the PtSnIr/C electrocatalyst prepared here with two times lower loading of Pt than PtSn/C E-tek electrocatalyst, it was possible to obtain the same maximum power density found for the commercial material. The main reaction product was acetic acid probably due to the presence of oxides, in this point the bifunctional mechanism is predominant, but an electronic effect should not be discarded.

Keywords: PtSnIr , ethanol oxidation reaction, electrocatalysis, nanostructured materials, fuel cells

Introduction

Polymeric exchange membrane fuel cells (PEMFCs) have been extensively studied due to their mobile, stationary and portable applications.[1,2] Among the PEMFCs, direct alcohol fuel cells (DAFCs) have the advantage that the liquid fuel can be more easily stored and handled compared to hydrogen.[3]

Ethanol is a more attractive fuel alcohol for PEMFC applications when compared with methanol because it is much less toxic, can be produced at a large scale from agricultural products or biomass,[4,5] and is more energetic (8 kWh kg^{-1} vs. 6.1 kWh kg^{-1}).[6] For these reasons, direct ethanol fuel cells (DEFCs) should achieve similar performance levels as direct methanol fuel cells.

However, the complete electrooxidation of ethanol is a 12-electron process, which is a practical challenge for the effectiveness of the catalysts. Pt is the most used metal for

*e-mail: mauro.santos@ufabc.edu.br

the oxidation of this alcohol, and its electrocatalytic activity can be improved by the addition of other metals such as Ru,[7-10] Sn,[8,10-13] Rh[14,15] and Ce.[16,17] However, these metals need to break the C–C bond at low temperatures,[5,18] and generate CO_2.[8,19] Thus, the investigation of the catalytic capacity of these materials in the ethanol oxidation process has become a priority.

Metallic iridium and IrO_2 are used as catalysts for oxygen evolution and reduction reactions in regenerative polymer electrolyte fuel cells.[20,21] The authors described that IrO_2 has high activity towards CO_{ads} electrooxidation. Moreover, these catalysts also exhibit excellent performance in the electrocatalysis of methanol in direct methanol fuel cells (DMFCs).[22,23] Chen *et al.*[24] showed that a thin layer of IrO_2 on $Ti/IrO_2/Pt$ improved the activity of these electrodes for methanol electrooxidation. They demonstrated that the current density increased and that the onset potential for methanol electrooxidation also shifted over 200 mV downward compared to the Ti/Pt nanoparticles. Additionally, iridium oxide exhibits good corrosion resistance in acid medium toward oxygen evolution.

Other studies have shown that the incorporating IrO_2 into Pt/C or PtRu/C can reduce the potential values for ethanol electrooxidation.[25] Ribeiro *et al.*[1] found out that the addition of iridium to Pt/C and PtSn/C catalysts can lead to higher electrocatalytic activity for ethanol oxidation. Cao *et al.*[26] demonstrated the high activity of Ir/C and Ir_3Sn/C for ethanol electrooxidation. In DEFC experiments, the Ir/C catalyst displayed performance similar to Pt/C, and Ir_3Sn/C showed activity similar to Pt_3Sn/C. This finding indicates that Ir is an excellent candidate to substitute or reduce the amount of Pt in electrocatalysts. Nevertheless, IrO_2 is extensively used in the preparation of mixed oxide electrodes, and numerous reports have suggested the application of Ir and its oxides in fuel cell systems.[22,27-29]

Indeed, results obtained through *in situ* Fourier transform infrared (FTIR) studies for ethanol electrooxidation on Ir electrodes[30] (Pt electrodes containing some Ir or its oxides and quaternary electrocatalysts) showed that these systems perform well for ethanol oxidation in a direct ethanol fuel cell.

Considering these results, it is evident that the presence of Ir in the electrocatalyst has a synergetic effect (generally with Pt) for both ethanol oxidation and direct ethanol fuel cell performance. Therefore, the aim of this work is to produce an optimized PtSnIr/C electrocatalyst, prepared by polymeric precursor method, to be used for both ethanol oxidation and as anode in a direct ethanol fuel cell. The main goals are to reduce the Pt content and to better understand the role of Ir in the ethanol oxidation reaction.

Experimental

Preparation of PtSnIr/C electrocatalysts

The PtSnIr/C electrocatalyst with a Pt:Sn:Ir atomic ratio of 1:1:1 was prepared by the polymeric precursor method reported by De Souza *et al.*[13,16,31]. For this purpose, a mass ratio of 1:50:400 (metallic precursor:citric acid (CA):ethylene glycol (EG)) was used to prepare the polymeric resin. Chloroplatinic acid ($H_2PtCl_6·6H_2O$, Sigma-Aldrich), tin chloride ($SnCl_2·2H_2O$, Merck) and iridium chloride were used as metallic precursors. The prepared polymeric resin was stored under refrigeration. The catalyst was prepared by placing a pre-determined volume of resin in an appropriate amount of carbon Vulcan XC-72 (Cabot Corporation) to give a total metal loading of 20 wt.%, followed by the addition of a sufficient amount of EG to cover the carbon powder. The pre-determined volume of resin was chosen to yield a final product containing equal atomic contents of Pt, Sn and Ir. The mixture was homogenized in an ultrasonic bath for 60 min and then thermally treated at 400 °C for 2 h in a N_2 atmosphere.

Material characterization

The catalyst morphology and particle sizes were obtained using JEOL 3010 HR-TEM (high resolution transmission electron microscopy) and JEOL JSM-5900LV microscopes. X-ray diffraction (XRD) patterns of the catalyst samples were recorded in a Rigaku Miniflex diffractometer using Cu K_α radiation (1.5406 Å, 30 kV and 15 mA). XPS measurements were carried out using a commercial spectrometer (UNI-SPECS UHV). The Mg K_α line was used (hv = 1253.6 eV), and the analyzer pass energy was set to 10 eV. The inelastic background of the C 1s, O 1s, Ir 4f, Pt 4f and Sn 3d electron core-level spectra was subtracted using Shirley's method. The binding energies of the spectra were corrected using the hydrocarbon component of adventitious carbon, fixed at 285.0 eV. The composition of the carbon-supported catalyst was determined from the ratios of the relative peak areas, corrected by sensitivity factors for the corresponding elements. The spectra were fitted without placing constraints using multiple Voigt profiles. The width at half maximum (FWHM) varied between 1.2 and 2.0 eV, and the accuracy of the peak positions was ± 0.1 eV.

Electrocatalyst activity characterization

In a single direct ethanol cell, the tested electrocatalyst anodes were PtSnIr/C and PtSn/C E-tek 20 wt.%, whereas

Pt/C E-tek 20 wt.% was used as cathode in the gas diffusion electrodes. The electrocatalyst was painted over the GDL (carbon cloth Teflon treated Electrochem ECCC1-060T) in the form of a homogeneous dispersion prepared using Nafion® solution (5 wt.%, Aldrich) and isopropanol (J. T. Baker). All electrodes contained 1 mg of Pt *per* cm^2 in the anode or in the cathode, except for PtSnIr/C, which contained 1 mg of Pt and Ir *per* cm^2. After the preparation, the electrodes were hot pressed on both sides of a Nafion® 117 membrane at 100 ºC for 2 min under a pressure of 225 kgf cm^{-2}. Prior to use, the membranes were exposed to 3 wt.% H_2O_2, thoroughly washed with distilled water and treated with 0.5 mol L^{-1} H_2SO_4. The performance of the ethanol fuel cell containing each catalyst was determined in a single cell with an area of 5 cm^2. The temperature was set to 100 ºC for the fuel cell and 80 ºC for the oxygen humidifier. The fuel (2 mol L^{-1} ethanol aqueous solutions) was delivered at approximately 2 mL min^{-1}, the oxygen flow was set to 500 mL min^{-1}, and the pressure was kept at 2 bar. Polarization curves were obtained using a TDI RBL 488 electronic load. The polarization curves were plotted using the data obtained with the potential measured in function of the current collected by the dynamic load, each polarization curve was performed under constant condition of aqueous ethanol and O_2 flow. The potential was measured using a system consisting of a single cell connected to a dynamic load, that after a period of stabilization of the system running (approximately 2 h) it was turned on to dynamic load at maximum current. The potential and current were measured every 10 s by reducing the current of 0.1 A *per* step until the open circuit potential. These conditions are standard to single cell experiments.

Additionally, the cell mechanism was studied by electrochemical experiments with a Solartron SI 1287 in acid media using an aqueous solution of 0.1 mol L^{-1} HClO$_4$ plus ethanol at three concentrations (0.5, 1 and 2 mol L^{-1}). The preparation of the electrocatalyst film on the gold substrate was as follows. First, an electrocatalyst solution was prepared by dispersing 4 mg of electrocatalyst powder in 1 ml of water and mixing for 5 min in an ultrasonic bath. Then, 20 μl of Nafion® solution (5%) were added to the suspension and mixed again in an ultrasonic bath for 15 min. Aliquots of 60 μL of the dispersion fluid were pipetted on the surface (0.78 cm^2) of the gold support. Finally, the electrode was dried at 60 °C for 20 min and hydrated for 5 min in water. The electrochemical cell was purged for 15 min with N$_2$ before each experiment. The experiments were monitored using a Nexus 670 spectrometer (Nicolet) with an MCT (mercury cadmium telluride) detector. The experiments were carried out at controlled temperature (25 ± 1.0 °C). Reflectance spectra were collected as the

ratio of R/R$_0$, where R represents a spectrum at a given potential and R$_0$ is the spectrum collected at 0.05 V. Positive and negative bands represent the consumption and production of substances, respectively. The spectra were recorded from the average of 128 interferograms.

Results and Discussion

Figure 1 shows a representative TEM image of the PtSnIr/C electrocatalyst and a particle size histogram. The size distributions were obtained measuring more than 300 particles. The micrograph reveals that the nanometric metal particles have a relatively straight size distribution (Table 1) and are uniformly dispersed on the support. It is important to note that 100% of the particles are between 1 and 10 nm. The determined particle sizes are in agreement with those reported in the literature for the frequently used platinum-tin electrocatalysts.[32-35]
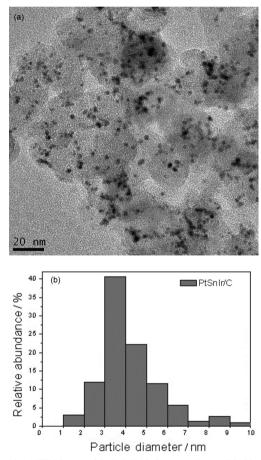

Figure 1. (a) TEM image of the PtSnIr/C electrocatalyst and (b) histogram of the catalyst mean particle diameter distribution over a size range of 0-10 nm.

Figure 2 displays the XRD patterns of the carbon-supported PtSnIr (1:1:1) ternary catalysts with a metal loading of 20 wt.%. For reference, the Pt (solid line), Ir

Table 1. Morphological information obtained from TEM images of the investigated catalysts

Electrocatalyst	Mean diameter / nm	Standard deviation / nm	Maximum diameter / nm	Minimum diameter / nm
PtSnIr/C	4.1	1.5	9.8	1.5

(dotted line) and IrO$_2$ (dashed line) peak patterns from cards JCPDF # 04-802, JCPDF # 87-715 and JCPDS # 06-0598, respectively, were inserted. Compared to the reflections in bulk Pt (220) with 2θ / 67.53°, the diffraction peak for the ternary catalyst is shifted to a lower 2θ value (66.93°). In fact, the peak pattern at 2θ / 66.93° is asymmetric, indicating the presence of more than one component, similar to the behavior already reported for PtSn,[36] PtCo[37] and PtRuIrSn[18] catalysts. In this work, Lorentzian lineforms[38] were used to deconvolute the four Bragg peaks located at 2θ / 39.44°, 45.85°, 66.93° and 80.03°.
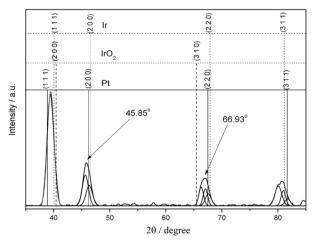

Figure 2. X-ray diffraction patterns of PtSnIr/C with the indicated peak patterns of Pt, Ir and IrO$_2$.

The peak at 2θ / 66.93° was decomposed into three main peaks centered at 66.28°, 67.08° and 67.58°, as shown in Figure 2. The lattice parameters of these three components are 0.39853, 0.39433 and 0.39175 nm, respectively. All three peaks displayed lattice parameter expansion due to lower 2θ values than those associated with Pt (0.39075 nm) and Ir (0.38977 nm). This suggests that Sn might be inserted into the Pt and/or Ir crystal structures as an alloy, as reported in several studies.[1,13,18,19,26] The third component at 2θ / 67.58° (0.39175 nm) is close to Pt (220) reflection (2θ / 67.53° and 0.39075 nm), suggesting the possible segregation of a fraction of Pt. This is supported by the presence of components at 2θ / 46.28° and 81.78° of the other two reflections at 2θ / 45.85° and 80.69° (Pt, 2θ / 46.27° and 81.37°). The possible segregation of a fraction of iridium (2θ / 81.09°) could be responsible for the component observed at 80.98° of the (311) reflection (2θ / 80.69°). There was no evidence for the presence of

crystalline SnO$_2$ and IrO$_2$, even though the existence of an amorphous phase cannot be ruled out.

The results obtained using X-ray diffraction analysis suggest a change in the electronic structure of PtSnIr compared to the pure metallic alloy constituents and a surface segregation of Pt and possibly also Ir.[39] Both phenomena could contribute to the electrocatalyst effects of our material discussed in the following sections.

To obtain further information of the characteristics of catalyst material, high resolution XPS spectra of Pt 4f, Ir 4f, Sn 3d, C 1s and O1s core levels were recorded. The results of the quantitative analysis indicate an equal atomic concentration of Pt and Sn. However, a lower Ir content than expected was obtained. The obtained element ratio of Pt:Sn:Ir was 1.0:1.0:0.3. This result indicates that the first mono-layers of the particle surface primarily consist of Pt and Sn phases. As shown in Figure 3a, the deconvoluted Pt 4f spectrum is formed by three spin-orbit doublets with the Pt 4f$_{7/2}$ components at 71.6, 72.3 and 74.3 eV, attributed to metallic Pt, Pt(OH)$_2$ and PtO$_2$ phases, respectively.[40] The lower intensity of the Ir 4f spectrum (Figure 3a) overlaps with the X-ray $\alpha_{3/4}$ Pt 4f satellites (peaks marked with black lines) making more difficulty the determination of the structural components for Ir. Consequently, despite the fact that binding energy of the fitted Ir 4f$_{7/2}$ component is 61.8 eV, close to the position expected for IrO$_2$, the presence of metallic iridium in the particles cannot be excluded. The Sn 3d$_{5/2}$ spectrum (Figure 3b) can be fitted with just one component, centered at 486.7 eV, indicating the coordination of tin with oxygen in the form of SnO$_2$.[40] The corresponding component was identified in the O 1s spectrum at 530.5 eV (not shown). Evidence of the formation of a Pt/Sn or Ir/Sn alloy could not be obtained due to the weak second neighbor interaction of Sn with Pt or Ir. The XPS results suggest the structure of the particles with a metallic core formed by Pt and Ir (or IrO$_2$) decorated by PtSnO$_2$ phase. The XPS results are key to the discussion of the electrocatalytical effect described in the next sections.

The performance in a real fuel cell is crucial for practical application. In Figure 4, an experiment with a single DEFC at 100 °C and with O$_2$ as the cathodic oxidant is presented. The performance obtained could effectively reflect the catalytic effect of the anode catalysts. The open-circuit voltage (OCV) of the DEFC is about 754 mV using the PtSnIr/C electrocatalysts as the anode, which is 18 mV lower than that obtained for the PtSn/C E-tek anode.
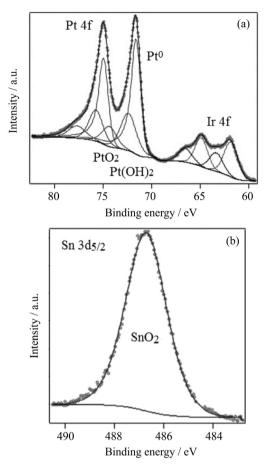
Figure 3. Fitted XPS core level spectra (a) Pt 4f and (b) Sn $3d_{5/2}$ of the PtSnIr/C catalyst.

Figure 4. Polarization and power density curves in a 5 cm² DEFC at 100 °C using (a) PtSnIr/C (1 $mg_{Pt + Ir}$ cm⁻²) or 20 wt.% PtSnIr/C and (b) PtSn/C E-tek as anode catalysts (1 mg_{Pt} cm⁻²) and 20 wt.% Pt/C E-tek as cathode catalyst (1 mg_{Pt} cm⁻²). Nafion® 117 was used as membrane.

However, the maximum power obtained using PtSnIr/C with half content of Pt is only slightly lower than that of the commercial material (31.5 mW cm⁻² vs. 32.0 mW cm⁻², respectively). To the best of our knowledge, these results have not been reported for a catalyst with reduced Pt content, as proposed here. Some promising results have been already discussed in the literature using PtSn/C, PtIr/C and PtSnIr/C.[1,41] However, these results were obtained using 40% metal loading on carbon. In fact, the high power density found here for a catalyst with half content of Pt, comparable to that obtained using a PtSn/C E-Tek anode, can be related to the presence of the main products generated during ethanol oxidation, as will be shown in the discussion of the FTIR results.

Figures 5a, 5b and 5c present the FTIR spectra of ethanol oxidation for three different ethanol concentrations (0.5, 1 and 2 mol L⁻¹) with increasing potential. They show the evolution of the bands associated with acetic acid (1280 cm⁻¹),[41] acetaldehyde (933 cm⁻¹)[15] and CO_2 (2343 cm⁻¹).[42] The presence of CO at lower potentials was reported for ethanol oxidation using *in situ* FTIR for PtSnIr/C electrocatalyts, though with 0.2 mol L⁻¹ ethanol and 40% of
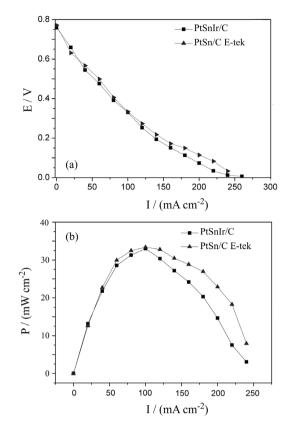
metal loading. In this work, it was not possible to observe the presence of CO, this is probably because of high ethanol concentration, when the ethanol concentration is increased the CO_2 decreased.[42,43] The absence of adsorbed CO could be indicating its easy removal from the surface of the catalysts through CO_2 formation.[1] Another aspect that must be taken into account is that the reflection-absorption theory of IR was developed to smooth surface and there are experimental evidences that heterogeneous surfaces can cause a noticeable reduction of the band intensities referent to adsorbed species and consequently, important information concerning CO is often lost when investigating such surfaces.[44] The results in this work may be indicative of the high conversion of ethanol to acetic acid and acetaldehyde for the ethanol concentrations used in this work, as found in a study using gas chromatography.[40] In Figures 5a, 5b and 5c, it can also be observed the interfacial water band close to 1600 cm⁻¹,[15] and the carbonyl band close to 1720 cm⁻¹.[45] It is important to stress that from a potential of 0.2 V, the formation of the products from ethanol oxidation can be verified.

To associate the changes with increasing or decreasing concentrations of specific species produced during the ethanol oxidation, all bands were deconvoluted by
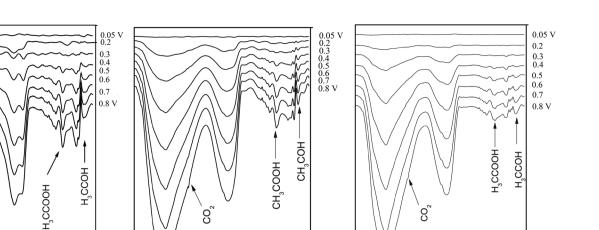
Figure 5. *In situ* FTIR spectra for a PtSnIr/C electrocatalyst in 0.1 mol L^{-1} HClO$_4$ in the presence of ethanol at concentrations of (a) 0.5, (b) 1 and (c) 2 mol L^{-1}. Reference spectra were taken at 0.05 V. Sample spectra measured after applying successive potential steps of 0.1 V, as indicated in the figure. Spectra were averaged from 128 scans. The spectral resolution was 8 cm^{-1} using a SeZn prismatic window.
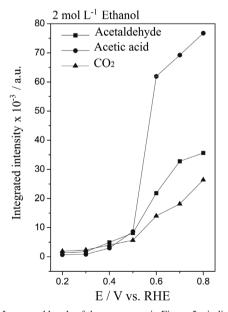
Lorentzian lineforms. Thus, in this study, the intensity and alignment of each band were individually analyzed as a function of the potential (Figure 6), an approach that has not been previously applied for *in situ* FTIR analysis during ethanol oxidation using PtSnIr/C electrocatalysts.
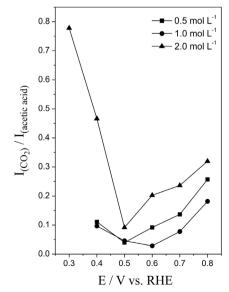

Figure 6. Integrated bands of the spectra set in Figure 5c, indicating the main products of ethanol oxidation.

The *in situ* FTIR integrated intensities for acetic acid, acetaldehyde and CO$_2$ on PtSnIr/C electrocatalyst (in 2 mol L^{-1} CH$_3$COOH and 0.1 mol L^{-1} HClO$_4$ solution)

are shown in Figure 6. It can be observed that the quantity of acetic acid, acetaldehyde and CO$_2$ increases with increasing electrocatalyst electrode potential. The acetic acid formation begins at about 0.4 V, whereas the CO$_2$ formation starts at 0.5 V.

Further investigations (presented in Figure 7) were performed examining the CO$_2$/acetic acid intensity ratio as a function of the electrode potential. The results show that the best efficiency related to the highest CO$_2$/acetic acid ratio was achieved in experiments using

Figure 7. The ratio of integrated intensities of CO$_2$ and acetic acid as a function of potential for the three ethanol concentrations in the solutions.

2 mol L^{-1} of ethanol. For 2 mol L^{-1} of ethanol, the PtSnIr/C electrocatalyst facilitates the production of CO_2 at low potentials. However, CO_2 formation rapidly decreases due to the faster formation of acetic acid, which agrees with the preferential oxidation route: ethanol to acetic acid rather than to CO_2. In contrast, for Pt/C,[46] this ratio is smaller at low potentials and reaches a maximum at about 650 mV. Additionally, when comparing the results obtained here for ethanol oxidation using PtSnIr/C with those using PtSn/C E-tek for the same process,[43] the latter catalyst displays a lower production of acetic acid in all potential regions and a higher production of CO_2.[43]

The interesting point here is the role of iridium as an electrocatalyst. Some authors[26,30] reported that iridium content in the electrocatalyst could favor acetaldehyde at low potentials when the surface was partially covered by CO_{ads} and H_{ads}. Furthermore, Gyenge *et al.*[47] revealed the favorable thermodynamics of OH_{ads} dissociation on Ir compared to Pt by the weak binding of H_2O to the Ir surface,[26,48] which also favors a bifunctional mechanism. Furthermore, the detection of a larger quantity of acetic acid (more oxidized species) in the product of the DEFC using a PtIrSn/C (20:5:15) anode is a further indication of the efficiency of the catalyst.[40] Consequently, the PtSnIr/C catalyst supports a mechanism in which the surface oxides facilitate the CO stripping of Pt atoms by providing oxygenated species for the CO (IrO_2 phase was identified using XPS). These oxygenated species can also react with ethanol or acetaldehyde adsorbed on the electrocatalyst producing acetic acid, i.e., a bifunctional mechanism.[49] However, an electronic effect cannot be excluded for two main reasons: (*i*) X-ray diffraction patterns indicated a change in the lattice parameter of Pt and/or Ir in the presence of Sn and (*ii*) because using XPS, the formation of a core-decorated with metal structure was suggested, and there are domains in which the electronic effect should be operating. Additionally, the core-decorated with metal structure evidenced by XPS can be an opened structure in which SnO_2 and IrO_2 are exposed and join with Pt, increasing the bifunctional mechanism.

Based on the reported data and the results discussed above, it can be concluded that IrO_2 facilitates a bifunctional mechanism incorporating both SnO_2 and Pt. In contrast, it is not possible to exclude an electronic effect either by the modification of the lattice parameters of Pt and Ir by the presence of Sn or the effect of a core-decorated with metal structure, as evidenced by XPS measurements. The presence of Ir helps to produce CO_2 at low potentials and also produces more acetic acid than CO_2 at higher potentials. Hence, it is possible to reduce the Pt content to half of that commonly used for the commercial PtSn/C material without any loss of power density of the fuel cell.

Conclusions

The PtSnIr/C electrocatalyst prepared by the polymeric precursor method presents a mixed system of different pure alloy phases or even a core-shell structure, such as shown from the results of XRD and XPS experiments. It was demonstrated that, in DEFC, the electrocatalyst displays performance similar to PtSn/C E-tek, however, with half content of platinum. The FTIR analysis of the ethanol oxidation showed that at lower potentials, acetaldehyde, acetic acid and CO_2 were the main reaction products involving very limited CO production. Based on the obtained results, it is evident that the utilization of Ir can considerably reduce Pt usage in the electrocatalyst, providing an equal power density compared to the commercial PtSn/C material.

Acknowledgments

References

1. Ribeiro, J.; dos Anjos, D. M.; Kokoh, K. B.; Coutanceau, C.; Léger, J. M.; Olivi, P.; de Andrade, A. R.; Tremiliosi-Filho, G.; *Electrochim. Acta* **2007**, *52*, 6997.

2. Li, H.; Sun, G.; Cao, L.; Jiang, L.; Xin, Q.; *Electrochim. Acta* **2007**, *52*, 6622.

3. Bergamaski, K.; Pinheiro, A. L. N.; Teixeira-Neto, E.; Nart, F. C.; *J. Phys. Chem. B* **2006**, *110*, 19271.

4. Hotza, D.; Costa, J. C. D.; *Int. J. Hydrogen Energy* **2008**, *33*, 4915.

5. Chang, Y.-W.; Liu, C.-W.; Wei, Y.-C.; Wang, K.-W.; *Electrochem. Commun.* **2009**, *11*, 2161.

6. Vigier, F.; Coutanceau, C.; Hahn, F.; Belgsir, E. M.; Lamy, C.; *J. Electroanal. Chem.* **2004**, *563*, 81.

7. Giz, M. J.; Camara, G. A.; Maia, G.; *Electrochem. Commun.* **2009**, *11*, 1586.

8. Wang, H.; Jusys, Z.; Behm, R. J.; *J. Power Sources* **2006**, *154*, 351.

9. Camara, G. A.; de Lima, R. B.; Iwasita, T.; *Electrochem. Commun.* **2004**, *6*, 812.

10. Colmati, F.; Antolini, E.; Gonzalez, E. R.; *J. Power Sources* **2006**, *157*, 98.

11. Zhou, W. J.; Li, W. Z.; Song, S. Q.; Zhou, Z. H.; Jiang, L. H.; Sun, G. Q.; Xin, Q.; Poulianitis, K.; Kontou, S.; Tsiakaras, P.; *J. Power Sources* **2004**, *131*, 217.

12. Silva, J. C. M.; De Souza, R. F. B.; Parreira, L. S.; Neto, E. T.; Calegaro, M. L.; Santos, M. C.; *Appl. Catal., B* **2010**, *99*, 265.

13. De Souza, R. F. B.; Parreira, L. S.; Rascio, D. C.; Silva, J. C. M.; Teixeira-Neto, E.; Calegaro, M. L.; Spinace, E. V.; Neto, A. O.; Santos, M. C.; *J. Power Sources* **2010**, *195*, 1589.

14. Kowal, A.; Gojkovic, S. L.; Lee, K. S.; Olszewski, P.; Sung, Y. E.; *Electrochim. Commun.* **2009**, *11*, 724.

15. Li, M.; Kowal, A.; Sasaki, K.; Marinkovic, N.; Su, D.; Korach, E.; Liu, P.; Adzic, R. R.; *Electrochim. Acta* **2010**, *55*, 4331.

16. De Souza, R. F. B.; Flausino, A. E. A.; Rascio, D. C.; Oliveira, R. T. S.; Neto, E. T.; Calegaro, M. L.; Santos, M. C.; *Appl. Catal., B* **2009**, *91*, 516.

17. Wang, J.; Xi, J.; Bai, Y.; Shen, Y.; Sun, J.; Chen, L.; Zhu, W.; Qiu, X.; *J. Power Sources* **2007**, *164*, 555.

18. Fatih, K.; Neburchilov, V.; Alzate, V.; Neagu, R.; Wang, H.; *J. Power Sources* **2010**, *195*, 7168.

19. Cao, L.; Sun, G.; Li, H.; Xin, Q.; *Fuel Cells Bull.* **2007**, *2007*, 12.

20. Ioroi, T.; Yasuda, K.; *J. Electrochem. Soc.* **2005**, *152*, A1917.

21. Ioroi, T.; Kitazawa, N.; Yasuda, K.; Yamamoto, Y.; Takenaka, H.; *J. Electrochem. Soc.* **2000**, *147*, 2018.

22. Sivakumar, P.; Tricoli, V.; *Electrochem. Solid-State Lett.* **2006**, *9*, A167.

23. Liang, Y. M.; Zhang, H. M.; Zhong, H. X.; Zhu, X. B.; Tian, Z. Q.; Xu, D. Y.; Yi, B. L.; *J. Catal.* **2006**, *238*, 468.

24. Chen, A. C.; La Russa, D. J.; Miller, B.; *Langmuir* **2004**, *20*, 9695.

25. Calegaro, M. L.; Suffredini, H. B.; Machado, S. A. S.; Avaca, L. A.; *J. Power Sources* **2006**, *156*, 300.

26. Cao, L.; Sun, G.; Li, H.; Xin, Q.; *Electrochem. Commun.* **2007**, *9*, 2541.

27. Birss, V. I.; Andreas, H.; Serebrennikova, I.; Elzanowska, H.; *Electrochem. Solid-State Lett.* **1999**, *2*, 326.

28. Liao, S. J.; Holmes, K. A.; Tsaprailis, H.; Birss, V. I.; *J. Am. Chem. Soc.* **2006**, *128*, 3504.

29. Tsaprailis, H.; Birss, V. I.; *Electrochem. Solid-State Lett.* **2004**, *7*, A348.

30. de Tacconi, N. R.; Lezna, R. O.; Beden, B.; Hahn, F.; Lamy, C.; *J. Electroanal. Chem.* **1994**, *379*, 329.

31. Polo, A. S.; Santos, M. C.; de Souza, R. F. B.; Alves, W. A.; *J. Power Sources* **2011**, *196*, 872.

32. Purgato, F. L. S.; Olivi, P.; Léger, J. M.; de Andrade, A. R.; Tremiliosi-Filho, G.; Gonzalez, E. R.; Lamy, C.; Kokoh, K. B.; *J. Electroanal. Chem.* **2009**, *628*, 81.

33. Colmati, F.; Antolini, E.; Gonzalez, E. R.; *Electrochim. Acta* **2005**, *50*, 5496.

34. Jiang, L.; Sun, G.; Zhou, Z.; Zhou, W.; Xin, Q.; *Catal. Today* **2004**, *93-95*, 665.

35. Zhu, M.; Sun, G.; Li, H.; Cao, L.; Xin, Q.; *Chin. J. Catal.* **2008**, *29*, 765.

36. García-Rodríguez, S.; Somodi, F.; Borbáth, I.; Margitfalvi, J. L.; Peña, M. A.; Fierro, J. L. G.; Rojas, S.; *Appl. Catal., B* **2009**, *91*, 83.

37. Aricò, A. S.; Shukla, A. K.; Kim, H.; Park, S.; Min, M.; Antonucci, V.; *Appl. Surf. Sci.* **2001**, *172*, 33.

38. Allmann, R. In *Powder Diffraction: Theory and Practice*; Dinnebier, R. E., Billinge, S. J. L., eds.; The Royal Society of Chemistry: Cambridge, 2008.

39. Demirci, U. B.; *J. Power Sources* **2007**, *173*, 11.

40. Moulder, J. F.; Stickle, W. F.; Sobol, P. E.; Bomben, K. D.; *Handbook of X-ray Photoelectron Spectroscopy*; Ed. J. Chastain, Perkin-Elmer Corporation, Physical Electronics Division, Eden Prairie, Minnesota, USA, 1992.

41. Tayal, J.; Rawat, B.; Basu, S.; *Int. J. Hydrogen Energy* **2011**, *36*, 14884.

42. Camara, G. A.; Iwasita, T.; *J. Electroanal. Chem.* **2005**, *578*, 315.

43. De Souza, R. F. B.; Parreira, L. S.; Silva, J. C. M.; Simões, F. C.; Calegaro, M. L.; Giz, M. J.; Camara, G. A.; Neto, A. O.; Santos, M. C.; *Int. J. Hydrogen Energy* **2011**, *36*, 11519.

44. Lima, R. B. ; Paganin, V.; Iwasita, T.; Vielstich, W.; *Electrochim. Acta* **2003**, *52*, 81.

45. Xia, X. H.; Liess, H. D.; Iwasita, T.; *J. Electroanal. Chem.* **1997**, *437*, 233.

46. Lima, F. H. B.; Gonzalez, E. R.; *Electrochim. Acta* **2008**, *53*, 2963.

47. Gyenge, E.; Atwan, M.; Northwood, D.; *J. Electrochem. Soc.* **2006**, *153*, A150.

48. Kua, J.; Goddard, W. A.; *J. Am. Chem. Soc.* **1999**, *121*, 10928.

49. Tong, Y. Y.; Kim, H. S.; Babu, P. K.; Waszczuk, P.; Wieckowski, A.; Oldfield, E.; *J. Am. Chem. Soc.* **2002**, *124*, 468.